Geosci. Model Dev. Discuss., 8, 3745–3790, 2015
www.geosci-model-dev-discuss.net/8/3745/2015/
doi:10.5194/gmdd-8-3745-2015
© Author(s) 2015. CC Attribution 3.0 License.

Geoscientific Model Development Discussions
Open Access

This discussion paper is/has been under review for the journal Geoscientific Model Development (GMD). Please refer to the corresponding final paper in GMD if available.

PLUME-MoM 1.0: a new 1-D model of volcanic plumes based on the method of moments

M. de' Michieli Vitturi[1], A. Neri[1], and S. Barsotti[2]

[1]Istituto Nazionale di Geofisica e Vulcanologia, Sezione di Pisa, Italy
[2]Icelandic Meteorological Office, Reykjavík, Iceland

Received: 27 March 2015 – Accepted: 17 April 2015 – Published: 5 May 2015

Correspondence to: M. de' Michieli Vitturi (mattia.demichielivitturi@ingv.it)

Published by Copernicus Publications on behalf of the European Geosciences Union.

Abstract

In this paper a new mathematical model for volcanic plumes, named PlumeMoM, is presented. The model describes the steady-state 1-D dynamics of the plume in a 3-D coordinate system, accounting for continuous variability in particle distribution of the pyroclastic mixture ejected at the vent. Volcanic plumes are composed of pyroclastic particles of many different sizes ranging from a few microns up to several centimeters and more. Proper description of such a multiparticle nature is crucial when quantifying changes in grain-size distribution along the plume and, therefore, for better characterization of source conditions of ash dispersal models. The new model is based on the method of moments, which allows description of the pyroclastic mixture dynamics not only in the spatial domain but also in the space of properties of the continuous size-distribution of the particles. This is achieved by formulation of fundamental transport equations for the multiparticle mixture with respect to the different moments of the grain-size distribution. Different formulations, in terms of the distribution of the particle number, as well as of the mass distribution expressed in terms of the Krumbein log scale, are also derived. Comparison between the new moments-based formulation and the classical approach, based on the discretization of the mixture in N discrete phases, shows that the new model allows the same results to be obtained with a significantly lower computational cost (particularly when a large number of discrete phases is adopted). Application of the new model, coupled with uncertainty quantification and global sensitivity analyses, enables investigation of the response of four key output variables (mean and standard deviation (SD) of the grain-size distribution at the top of the plume, plume height and amount of mass lost by the plume during the ascent) to changes in the main input parameters (mean and SD) characterizing the pyroclastic mixture at the base of the plume. Results show that, for the range of parameters investigated, the grain-size distribution at the top of the plume is remarkably similar to that at the base and that the plume height is only weakly affected by the parameters of the grain distribution.

GMDD
8, 3745–3790, 2015

1 Introduction

In the past decades, numerical simulation of volcanic eruptions has greatly advanced and models are now often able to deal with the multiphase nature of volcanic flows. This is the case, for example, of models describing the dynamics of pyroclastic particles in a volcanic plume, or that of bubbles and crystals dispersed in the magma rising in a volcanic conduit. Despite this, in numerical models, the polydispersity associated with the multiphase nature of volcanic flows is often ignored or largely simplified. For instance, in most of the existing conduit models, crystals and bubbles are treated as simple flow components and described by volume fractions only, while in plume dynamics and ash dispersal models the grain size distribution of pyroclasts is discretized in a finite number of classes (i.e. phases). Both approaches make proper treatment of the continuous variability of fundamental physical and chemical properties of the dispersed phases, for instance, the dimension of pyroclastic particles and gas bubbles difficult. Literature results clearly show that this variability can largely affect relevant physical/chemical processes that occur during the transport of the dispersed phase such as, for example, the nucleation and growth of bubbles and the coalescence/breakage of bubbles and crystals in the conduit or the aggregation of pyroclastic particles in a volcanic plume. Recently, a theoretical framework and the corresponding computational models, namely the method of moments for disperse multiphase flows, have been developed, mostly in the chemical engineering community (Hulburt and Katz, 1964; Marchisio et al., 2003), to track the evolution of these systems not only in the physical space, but also in the space of properties of the dispersed phase (called internal coordinates). According to this method, a population balance equation is formulated as a continuity statement written in terms of a density function. From the density function transport equation some integral quantities of interest (namely the moments) are then derived and their transport equations are formulated. In this work we present an extension of the Eulerian steady-state volcanic plume model presented in Barsotti et al. (2008) (derived from Bursik, 2001) obtained by adopting the method of

GMDD
8, 3745–3790, 2015

moments. In contrast to the original works where pyroclastic particles are partitioned into a finite number of classes with different size and properties, the new model is able to consider a continuous size distribution function of pyroclasts, $f(D)$, representing the number or the mass fraction of particles (for unit volume) with diameter between D and $D + \mathrm{d}D$. Accordingly, transport equations of the plume are expressed in terms of the transport equations for the moments of the ash particles size distribution. In this work we present the new multiphase model formulation based on the implementation of the quadrature and we investigate the sensitivity of the model to uncertain or variable input parameters such as those describing the grain-size distribution of the mixture. To quantify and incorporate uncertainty into our application of the model we tested two different approaches, a modification of the Monte Carlo method based on Latin hypercube sampling and a stochastic approach, namely the generalized Polynomial Chaos Expansion method.

This paper is organized as follows: in Sect. 2 we present the method of moments applied to two different descriptions of particles distribution. In Sect. 3 the equations of the model for the two formulations are described. Section 4 is devoted to the numerical discretization of the model and the numerical implementation of the method of moments. Section 5 presents the application of the model to three test cases with a comparison of the model results for different formulations of the plume model, and finally an uncertainty quantification and a sensitivity analysis are applied to model results.

2 Method of moments

2.1 Moments of the size distribution

In contrast to previous works, where the solid particles are partitioned in a finite number of classes with different size, we introduce here a continuous size distribution function representing the number (or mass) concentration of particles (for unit volume) as

GMDD
8, 3745–3790, 2015

a function of the particles diameter. In general, this particle size distribution (PSD) is a function of time t, of the spatial coordinate and of the diameter of the particles.

First, we present the method of moments for a particle size distribution $f(D)$, representing the number concentration of particles (particles for unit volume) with diameter between D and $D + \mathrm{d}D$, where D is expressed in meters. When more than one family of particles are present, for example lithics and pumice, we will use the subscript j to distinguish among them. Consequently, the function $f_j(D)$ will denote the number concentration of particles of the jth family.

Given a particle size distribution $f_j(D)$, we observe that its "shape" can be quantified through the moments $M_j^{(i)}$ (Hazewinkel, 2001), defined by

$$M_j^{(i)} = \int_0^{+\infty} D^i f_j(D)\mathrm{d}D. \tag{1}$$

The particular definition of $f_j(D)$ we adopt, expressing the number concentration of particles of size D, allows the following physical interpretation of the first four moments:

- $M_j^{(0)}$ is total number of particles of the jth family (per unit volume);
- $M_j^{(1)}$ is sum of the particles diameter of the jth family (per unit volume);
- $M_j^{(2)}$ is total surface area of particles of the jth family (per unit volume);
- $\frac{\pi}{6}M_j^{(3)}$: total volume of particles of the jth family (per unit volume) or the local volume fraction of the jth dispersed phase, also denoted with $\alpha_{s,j}$.

Furthermore, a mean particle size can be defined as the ratio of the moments $M_j^{(i+1)}/M_j^{(i)}$ for any value of i. For example, the Sauter mean diameter is defined by

GMDD
8, 3745–3790, 2015
PLUME-MoM
M. de' Michieli Vitturi et al.

CC BY

setting $i = 2$, giving $L_{j,32} = M_j^{(3)}/M_j^{(2)}$. Similarly, it is possible to define the mean particle length averaged with respect to particle number density $L_{j,10} = M_j^{(1)}/M_j^{(0)}$, i.e. the sum of the lengths of particles per unit volume divided by the number of particles, and the mean particle length averaged with respect to particle volume-fraction density function $L_{j,43} = M_j^{(4)}/M_j^{(3)}$.

The motivation for the introduction of the moments is to minimize computational costs by avoiding the discretization of the size distribution in several classes, and nevertheless to capture the polydispersity of the flow through the correct description of the evolution of the moments (Carneiro, 2011). The moments and the corresponding transport velocities appear naturally in the mathematical formulation as a direct consequence of the integration of the Eulerian particle equations over the diameter spectrum, as will be shown in the next section.

2.2 Moments of other quantities

In the plume model, several quantities characteristic of the particles, as settling velocity, density and specific heat capacity, are also defined as function of the particle diameter, and thus we can define their moments as done for the distribution $f_j(D)$. In general, for a quantity ψ_j function of the diameter D, we define its moments as

$$\psi_j^{(i)} = \frac{1}{M_j^{(i)}} \int_0^{+\infty} \psi_j(D) D^i f_j(D) \mathrm{d}D. \tag{2}$$

As a first example, we consider here the moments of particles density ρ_s. In particular, following Bonadonna and Phillips (2003), density of lithics is assumed to be constant, whereas density of pumices with diameter $D < D_2$ is assumed to decrease linearly and to reach the lithic density value when the fragment diameter decreases

GMDD
8, 3745–3790, 2015

below D_1:

$$\rho_{s,\mathrm{pum}}(D) = \begin{cases} \rho_1 & D < D_1 \\ \rho_1 + \frac{D-D_1}{D_2-D_1}(\rho_2 - \rho_1) & D_1 \le D \le D_2 \\ \rho_2 & D > D_2 \end{cases} \tag{3}$$

Substituting the expression for the particles density of the jth particle family in Eq. (2), we obtain the moments of the density as:

$$\rho_{s,j}^{(i)} = \frac{1}{M_j^{(i)}} \int_0^{+\infty} \rho_{s,j}(D) D^i f_j(D) \mathrm{d}D. \tag{4}$$

We remark that moments of different order are generally different, they will only be equal ($\rho_{s,j}^{(l)} = \rho_{s,j}^{(m)}$, $l \neq m$) in two limiting cases: for a monodisperse distribution, i.e. $f_j(D) = \delta(D - D^*)$, with $\rho_{s,j}(D^*) = \rho_s^*$; or if all particles have the same density, i.e. $\rho_{s,j}(D) = \rho_{s,j}^*$, $\forall D$. In both cases, $\rho_{s,j}^{(i)} = \rho_{s,j}^*$, $\forall i$. Otherwise, there is no reason, e.g., for $\rho_{s,j}^{(1)}$ and $\rho_{s,j}^{(3)}$ to be the same, as they represent length and volume weighted density averages, respectively. For our application, we are interested mostly in the volumetric averaged density $\rho_{s,j}^{(3)}$, i.e. the mass of particles per unit volume from now on denoted with $\tilde{\rho}_{s,j}$.

The moments defined by Eq. (4) can also be used to define other properties of the gas-particles mixture. For example, it follows from the definition of the moments that if we have a mixture of a gas with density ρ_g and a family of polydisperse distributions of particles with density $\rho_{s,j} = \rho_{s,j}(D)$, the mixture density is given by:

$$\rho_\mathrm{mix} = \sum_j \alpha_{s,j} \tilde{\rho}_{s,j} + \left(1 - \sum_j \alpha_s\right) \rho_\mathrm{g} = \sum_j \frac{\pi}{6} M_j^{(3)} \rho_{s,j}^{(3)} + \left(1 - \sum_j \frac{\pi}{6} M_j^{(3)}\right) \rho_\mathrm{g} \tag{5}$$

GMDD
8, 3745–3790, 2015

and consequently the mass fraction of the jth solid phase with respect to the gas-particles mixture is given by:

$$x_{s,j} = \frac{\alpha_{s,j}\widetilde{\rho}_{s,j}}{\rho_{\mathrm{mix}}} = \frac{\frac{\pi}{6}M_j^{(3)}\rho_{s,j}^{(3)}}{\sum_j \frac{\pi}{6}M_j^{(3)}\rho_{s,j}^{(3)} + \left(1 - \sum_j \frac{\pi}{6}M_j^{(3)}\right)\rho_{\mathrm{g}}}. \tag{6}$$

We also remark that here the gas phase is a mixture of atmospheric air, entrained in the plume during the rise in the atmosphere, and a volcanic gas component, generally water vapour. In the following, we will use the subscript atm to denote the atmospheric air and wv for the volcanic water vapour.

Differently from the approach used in Barsotti et al. (2008), where the settling velocity for each class is provided by the user, here several models have implemented in the code Pfeiffer et al. (2005); Textor et al. (2006a, b). For the application presented in this work, the settling velocity is defined as a function of the particle diameter and density as in Textor et al. (2006a),:

$$w_{s,j}(D) = \begin{cases} k_1\left(\frac{D}{2}\right)^2 \rho_{s,j}(D)\sqrt{\frac{\rho_{\mathrm{atm}}^0}{\rho_{\mathrm{atm}}}} & D \le 10\,\mu\mathrm{m} \\ k_2\left(\frac{D}{2}\right)\rho_{s,j}(D)\sqrt{\frac{\rho_{\mathrm{atm}}^0}{\rho_{\mathrm{atm}}}} & 10 < D \le 10^3\,\mu\mathrm{m} \\ k_3\sqrt{\frac{D}{2}}\sqrt{\frac{\rho_{s,j}(D)}{C_D}}\sqrt{\frac{\rho_{\mathrm{atm}}^0}{\rho_{\mathrm{atm}}}} & D > 10^3\,\mu\mathrm{m} \end{cases} \tag{7}$$

Proceeding as done for the particle density, it is possible to evaluate the moments $w_{s,j}^{(i)}$ of the settling velocity $w_{s,j}(D)$, defined as

$$w_{s,j}^{(i)} = \frac{1}{M_j^{(i)}}\int_0^{+\infty} w_{s,j}(D)D^i f_j(D)\mathrm{d}D \tag{8}$$

GMDD
8, 3745–3790, 2015

and representing weighted integrals of the settling velocity over the size spectrum. Again, moments of different order are generally different. There is no reason, e.g., for $w_{s,j}^{(2)}$ and $w_{s,j}^{(3)}$ to be the same, as they represent surface and volume weighted averages, respectively.

Finally, it is possible to define the moments $C_{s,j}^{(i)}$ of the particles specific heat capacity $C_{s,j}$:

$$C_{s,j}^{(i)} = \frac{1}{M_j^{(i)}} \int_0^{+\infty} C_{s,j}(D) D^i f_j(D) \mathrm{d}D. \tag{9}$$

We observe that for the specific heat capacity generally we are not interested in a volumetric average but in the mass average, denoted here with the notation $\overline{C}_{s,j}$ and given by the following expression:

$$\overline{C}_{s,j} = \int_0^{+\infty} C_{s,j}(D) \frac{\rho_{s,j}(D) D^3}{\widetilde{\rho}_{s,j} M_j^{(3)}} f_j(D) \mathrm{d}D = \frac{1}{\widetilde{\rho}_{s,j}} \left[C_{s,j} \rho_{s,j} \right]^{(3)}. \tag{10}$$

2.3 Mass fraction distribution

While in chemical engineering, where the method of moments is commonly used, the particle number distribution $f_j(D)$ is generally preferred to describe the polidispersity of the particles, in volcanology it is more common to use a mass fraction distribution $\varphi_j(\phi)$, defined as a function of the Krumbein phi (ϕ) scale:

$$\phi = -\log_2 \frac{1000D}{D_0},$$

where D is the diameter of the particle expressed in meters, and D_0 is a reference diameter, equal to 1 mm (to make the equation dimensionally consistent).

GMDD
8, 3745–3790, 2015

In this case, the distribution $\varphi_j(\phi)$ represents the mass fraction of particles (mass per unit mass of the gas-particles mixture) of the jth family with diameter between ϕ and $\phi + \mathrm{d}\phi$. Again, the shape of the distribution $\varphi_j(\phi)$ can be characterized by its moments $\Pi_j^{(i)}$, defined by

$$\Pi_j^{(i)} = \int_{-\infty}^{+\infty} \phi^i \varphi_j(\phi) \mathrm{d}\phi. \tag{11}$$

Also in this case the particular definition of $\varphi_j(\phi)$ allows a physical interpretation of the moments: for example, the moment $\Pi_j^{(0)}$ is the mass fraction of the jth solid phase $x_{s,j}$ with respect to the gas-particles mixture. As done with the particles number distribution, it is possible to define a mean particle size in terms of the moments of the mass fraction distribution as $\Pi_j^{(i+1)}/\Pi_j^{(i)}$; this ratio, for $i = 0$, gives the mass averaged diameter, corresponding to the volume averaged diameter $L_{j,43} = M_j^{(4)}/M_j^{(3)}$ when the density $\rho_{s,j}(\phi)$ is constant.

Again, it is possible to define the moments of other quantities $\psi_j(\phi)$ in terms of the continuous distribution of mass fraction $\varphi_j(\phi)$ as

$$\psi_j^{(i)} = \frac{1}{\Pi_j^{(i)}} \int_{-\infty}^{+\infty} \psi_j(\phi) \phi^i \varphi_j(\phi) \mathrm{d}\phi. \tag{12}$$

For example, when the mass fraction distribution $\varphi_j(\phi)$ is used, the mass averaged heat capacity $\overline{C}_{s,j}$ is given by the following expression:

$$\overline{C}_{s,j} = \int_{-\infty}^{+\infty} C_{s,j}(\phi) \frac{\varphi_{s,j}(\phi)}{x_{s,j}} \mathrm{d}\phi = \frac{1}{\Pi_j^{(0)}} \left[C_{s,j}\right]^{(0)} \tag{13}$$

GMDD
8, 3745–3790, 2015

and the volumetric averaged density, i.e. the mass of particles per unit volume, can be evaluated from

$$\frac{1}{\widetilde{\rho}_{s,j}} = \frac{1}{x_{s,j}} \int_{-\infty}^{+\infty} \frac{\varphi_{s,j}(\phi)}{\rho_{s,j}(\phi)} \mathrm{d}\phi = \frac{1}{\Pi_j^{(0)}} \left[\frac{1}{\rho_{s,j}}\right]^{(0)}. \tag{14}$$

3 Plume model

The equation set for the plume rise model is solved in a 3-D coordinate system (s, ϕ, θ) by considering the bulk properties of the eruptive mixture (see Fig. 1). The plume is assumed with a circular section along the curvilinear coordinate s, an inclination on the ground defined by an angle ϕ between the axial direction and the horizon, and an angle θ in the horizontal plane (x, y) with respect to the x axis. This last feature is needed to describe the evolution of weak explosive eruptions which are strongly affected by atmospheric conditions.

Following Bursik (2001) and Ernst et al. (1996), the conservation of flux of particles with size D of the jth family is given by:

$$\frac{\mathrm{d}}{\mathrm{d}s}\left(f_j(D)\pi r^2 U_{\mathrm{sc}}\right) = -2\pi r p w_{s,j}(D) f_j(D) \tag{15}$$

where r is characteristic plume radius, U_{sc} represents the velocity of the plume cross section along its centerline and p is a probability that an individual particle will fall out of the plume, defined as a function of an entrainment coefficient α (see below)

$$p = \frac{\left(1 + \frac{6}{5}\alpha\right)^2 - 1}{\left(1 + \frac{6}{5}\alpha\right)^2 + 1}. \tag{16}$$

Equation (15) states that the number of particles of the jth family with size D lost from the plume is proportional to the number of particles at the plume margin, given by $f_j(D) \cdot 2\pi r$, to the settling velocity $w_{s,j}(D)$ and to the probability factor p.

GMDD
8, 3745–3790, 2015

Now, multiplying both the sides of Eq. (15) for D^i and then integrating over the size spectrum $[0, +\infty]$, we obtain the following conservation equations for the moments $M_j^{(i)}$:

$$\frac{\mathrm{d}}{\mathrm{d}s}\left(M_j^{(i)} U_{\mathrm{sc}} r^2\right) = -2rpw_{s,j}^{(i)} M_j^{(i)}. \tag{17}$$

If we compare our formulation with that presented in Barsotti et al. (2008), where the effects of a polydisperse solid phase are taken into account partitioning the size spectrum in a finite number N of solid classes, the set of Eq. (17) replaces the N mass conservation equations for the N particulate classes.

From Eq. (15), if we multiply both the terms for the mass of the particles of size D, given by $\frac{\pi}{6}D^3\rho_j(D)$, we obtain the additional equation:

$$\frac{\mathrm{d}}{\mathrm{d}s}\left(f_j(D)\frac{\pi}{6}D^3\rho_j(D)\pi r^2 U_{\mathrm{sc}}\right) = -2\pi rpw_{s,j}(D)f_j(D)\frac{\pi}{6}D^3\rho_j(D) \tag{18}$$

and, integrating over the size spectrum:

$$\frac{\mathrm{d}}{\mathrm{d}s}\left(U_{\mathrm{sc}} r^2 \frac{\pi}{6} M_j^{(3)} \rho_j^{(3)}\right) = -2rp\frac{\pi}{6}M^{(3)}\left[w_{s,j}\rho_{s,j}\right]^{(3)}, \tag{19}$$

where on the left hand-side the term $\frac{\pi}{6}M_j^{(3)}\rho_j^{(3)}$ represents the volume average bulk density of the particles of the jth family, while on the right-hand side the term $\left[w_{s,j}\rho_{s,j}\right]^{(3)}$ represents the mass averaged settling velocity of the particles of the jth family multiplied by the volume averaged particles density. Equation (19) is the mass conservation equation for the jth family of particles, relating the variation of the mass flux of particles within the plume with the loss at the plume margin.

Now, following the same procedure, we want to reformulate the other conservation equations describing the steady-state ascent of the plume in terms of the moments of the continuous distributions of sizes, densities and settling velocities instead of the averages over a finite number of classes of particles with different size.

GMDD
8, 3745–3790, 2015

First of all, we derive the conservation equation for the mixture mass. As in the plume theory, we assume that the entrainment, due to both turbulence in the rising buoyant jet and to the crosswind field, is parameterized through the use of two entrainment coefficients, α and γ. The theory assumes that the efficiency of mixing with ambient air is proportional to the product of a reference velocity (the vertical plume velocity in one case and the wind field component along the plume centerline in the other), by α and γ (Morton, 1959; Briggs, 1975; Wright, 1984; Weil, 1988). Thus, following Bursik (2001), we define the entrainment velocity U_e as a function of windspeed, U_{atm}, as well as axial plume speed, U_{sc}:

$$U_e = \alpha|U_{\mathrm{sc}} - U_{\mathrm{atm}}\cos\phi| + \gamma|U_{\mathrm{atm}}\sin\phi| \tag{20}$$

where $\alpha|U_{\mathrm{sc}} - U_{\mathrm{atm}}\cos\phi|$ is entrainment by radial inflow minus the amount swept tangentially along the plume margin by the wind, and $\gamma|U_{\mathrm{atm}}\sin\phi|$ is entrainment from wind. With this notation, the total mass conservation equation solved by the model becomes

$$\frac{\mathrm{d}}{\mathrm{d}s}\left(\rho_{\mathrm{mix}}U_{\mathrm{sc}}r^2\right) = 2r\rho_{\mathrm{atm}}U_e - 2rp\sum_j \frac{\pi}{6}M_j^{(3)}\left[w_{s,j}\rho_{s,j}\right]^{(3)}, \tag{21}$$

stating that the variation of mass flux (left-hand side term) is due to air entrainment (first right-hand side term) and loss of solid particles (second right-hand side term), as obtained from Eq. (19).

From the variation of mass flux, we can derive also the horizontal and vertical components of the momentum balance solved by the model as:

$$\frac{\mathrm{d}}{\mathrm{d}s}\left(\rho_{\mathrm{mix}}U_{\mathrm{sc}}r^2(u - U_{\mathrm{atm}})\right) = -r^2\rho_{\mathrm{mix}}w\frac{\mathrm{d}U_{\mathrm{atm}}}{\mathrm{d}z} - 2upr\sum_j \frac{\pi}{6}M_j^{(3)}\left[w_{s,j}\rho_{s,j}\right]^{(3)}, \tag{22}$$

and

$$\frac{\mathrm{d}}{\mathrm{d}s}\left(\rho_{\mathrm{mix}}U_{\mathrm{sc}}r^2w\right) = gr^2(\rho_{\mathrm{atm}} - \rho_{\mathrm{mix}}) - 2wpr\sum_j \frac{\pi}{6}M_j^{(3)}\left[w_{s,j}\rho_{s,j}\right]^{(3)}, \tag{23}$$

GMDD
8, 3745–3790, 2015

where the two components of plume velocity along the horizontal and vertical axes are u and w, respectively, and they are linked by the relation $U_{sc} = \sqrt{u^2 + w^2}$. In the right-hand side of Eq. (22) the terms related to the exchange of momentum due to the wind and to momentum loss from the fall of solid particles appear. Similar contributions are evident in the right-hand side term of Eq. (23) where the vertical momentum is changed by the gravitational acceleration term and the segregation of particles.

Now, following the notation adopted above and denoting with T the mixture temperature, the equation for conservation of thermal energy solved by the model writes as

$$\frac{\mathrm{d}}{\mathrm{d}s}\left(\rho_{\mathrm{mix}} U_{sc} r^2 C_{\mathrm{mix}} T\right) = 2r\rho_{\mathrm{atm}} U_e C_{\mathrm{atm}} T_{\mathrm{atm}} - r^2 w \rho_{\mathrm{atm}} g - 2Tpr \sum_j \frac{\pi}{6} M_j^{(3)} \left[C_{s,j} w_{s,j} \rho_{s,j}\right]^{(3)}. \tag{24}$$

The first term on right-hand side describes the cooling of the plume due to ambient air entrainment, the second one takes into account atmospheric thermal stratification, and the third term allows for heat loss due to loss of solid particles. Again, this last term is obtained writing the heat loss for the particles of size D, and then integrating over the size spectrum. A thermal equilibrium between solid and gaseous phases is assumed. In Eq. (24) C_{atm} and C_{mix} are the heat capacity of the entrained atmospheric air and of the mixture, respectively, the latter being defined as:

$$C_{\mathrm{mix}} = \left(1 - \sum_j x_{s,j}\right) C_{p,g} + \sum_j x_{s,j} \overline{C}_{s,j} \tag{25}$$

or, in terms of the bulk densities ρ^B_{atm}, ρ^B_{wv} and $\rho^B_{s,j} = \frac{\pi}{6} M_j^{(3)} \widetilde{\rho}_{s,j}$, as

$$C_{\mathrm{mix}} = \frac{\rho^B_{\mathrm{atm}} C_{\mathrm{atm}} + \rho^B_{\mathrm{wv}} C_{\mathrm{wv}} + \sum_j \rho^B_{s,j} \overline{C}_{s,j}}{\rho^B_{\mathrm{atm}} + \rho^B_{\mathrm{wv}} + \sum_j \rho^B_{s,j}}. \tag{26}$$

GMDD
8, 3745–3790, 2015

From this expression, if we multiply all the terms at the numerator and the denominator of the right-hand side by $U_{sc}r^2$ and we derive with respect to s, we obtain after some cancellation and algebra manipulations the following equation for the variation of the mixture specific heat with s:

$$\frac{\partial C_{mix}}{\partial s} = \frac{1}{\rho_{mix}U_{sc}r^2}\left[(C_{atm}-C_{mix})\frac{\partial}{\partial s}\left(\rho^B_{atm}U_{sc}r^2\right)+\sum_j\left(\overline{C}_{s,j}-C_{mix}\right)\frac{\partial}{\partial s}\left(\rho^B_{s,j}U_{sc}r^2\right)\right] + \sum_j\frac{\rho^B_{s,j}}{\rho_{mix}}\left[\frac{\frac{\partial}{\partial s}\left(\overline{C}_{s,j}\rho^B_{s,j}U_{sc}r^2\right)}{\rho^B_{s,j}U_{sc}r^2}-\frac{\overline{C}_{s,j}\frac{\partial}{\partial s}\left(\rho^B_{s,j}U_{sc}r^2\right)}{\rho^B_{s,j}U_{sc}r^2}\right]. \tag{27}$$

Now, substituting the expressions for the partial derivatives appearing in each term on the right-hand side, we obtain the equation for the variation rate of mixture specific heat in terms of the moments:

$$\frac{\partial C_{mix}}{\partial s} = \frac{1}{\rho_{mix}U_{sc}r^2}\left[C_{atm}2r\rho_{atm}U_e - C_{mix}\left(2r\rho_{atm}U_e - 2pr\sum_j\frac{\pi}{6}M^{(3)}_j\left[w_{s,j}\rho_{s,j}\right]^{(3)}\right) - 2pr\sum_j\frac{\pi}{6}M^{(3)}_j\left[w_{s,j}\rho_{s,j}C_{s,j}\right]^{(3)}\right] \tag{28}$$

Similarly, a gas constant R_g can be defined as a weighted average of the gas constant for the entrained atmospheric air R_{atm} and the gas constant of the volcanic water vapour R_{wv}

$$R_g = \frac{\rho^B_{atm}R_{atm}+\rho^B_{wv}R_{wv}}{\rho^B_{atm}+\rho^B_{wv}} \tag{29}$$

GMDD
8, 3745–3790, 2015

and a conservation equation can be derived, knowing that the variation of gaseous mass fraction with height is solely due to entrained air:

$$\frac{\partial R_g}{\partial s} = \frac{R_{atm} - R_g}{\rho_{mix}(1 - x_s)U_{sc}r^2} \cdot 2r\rho_{atm}U_e. \tag{30}$$

This formulation reduces, for particular cases, to the expressions of Woods (1988) and Glaze and Baloga (1996). Equations (28) and (30) are needed in order to close the system of equations and recover the new values of the temperature and the mixture density once the system of ordinary differential equations is integrated. Otherwise, to obtain for example the values of the temperature at $s + \mathrm{d}s$ from the lumped term $(\rho_{mix}U_{sc}r^2C_{mix}T)$ obtained integrating Eq. (38), we should use the values at s of ρ_{mix} and C_{mix}.

Finally, as in Bursik (2001), the equations expressing the coordinate transformation between (x, y, z) and (s, ϕ, θ) are given by:

$$\frac{\partial z}{\partial s} = \sin\phi, \quad \frac{\partial x}{\partial s} = \cos\phi\cos\theta, \quad \frac{\partial y}{\partial s} = \cos\phi\sin\theta. \tag{31}$$

3.1 Mass fraction distribution

Similarly as done for the distribution of particles number $f_j(D)$ and the moments $M_j^{(i)}$, it is possible to derive a set of conservation equations in terms of the moments $\Pi_j^{(i)}$ of the mass fraction distribution $\varphi_j(\phi)$ expressed as a function of the Krumbein scale.

In this case, the conservation of mass flux of particles with size ϕ of the jth family write as:

$$\frac{\mathrm{d}}{\mathrm{d}s}\left(\rho_{mix}\varphi_j(\phi)\pi r^2 U_{sc}\right) = -2\pi r\rho w_{s,j}(\phi)\rho_{mix}\varphi_j(\phi). \tag{32}$$

Multiplying both sides of the equation for ϕ^i and integrating over the size spectrum $[-\infty, +\infty]$, we obtain the following conservation equations for the moments of the con-

GMDD
8, 3745–3790, 2015

tinuous distributions $\varphi_j(\phi)$:

$$\frac{\mathrm{d}}{\mathrm{d}s}\left(\Pi_j^{(i)}\rho_{\mathrm{mix}}U_{\mathrm{sc}}r^2\right) = -2rp\rho_{\mathrm{mix}}w_{s,j}^{(i)}\Pi_j^{(i)}. \tag{33}$$

For $i = 0$, the equations of conservation of the moments give:

$$\frac{\mathrm{d}}{\mathrm{d}s}\left(x_{s,j}\rho_{\mathrm{mix}}U_{\mathrm{sc}}r^2\right) = -2rp\rho_{\mathrm{mix}}w_{s,j}^{(0)}x_{s,j} \tag{34}$$

expressing the loss of mass flux of the particles of the jth family and thus we can write the total mass conservation equation as

$$\frac{\mathrm{d}}{\mathrm{d}s}\left(\rho_{\mathrm{mix}}U_{\mathrm{sc}}r^2\right) = 2r\rho_{\mathrm{atm}}U_{\epsilon} - 2rp\rho_{\mathrm{mix}}\sum_j w_{s,j}^{(0)}\Pi_j^{(0)}. \tag{35}$$

From the variation of mass flux, as done for the distribution of particles number $f_j(D)$ and the moments $M_j^{(i)}$, we derive the horizontal and vertical components of the momentum balance:

$$\frac{\mathrm{d}}{\mathrm{d}s}\left(\rho_{\mathrm{mix}}U_{\mathrm{sc}}r^2(u-U_{\mathrm{atm}})\right) = -r^2\rho_{\mathrm{mix}}w\frac{\mathrm{d}U_{\mathrm{atm}}}{\mathrm{d}z} - 2upr\rho_{\mathrm{mix}}\sum_j w_{s,j}^{(0)}\Pi_j^{(0)}, \tag{36}$$

$$\frac{\mathrm{d}}{\mathrm{d}s}\left(\rho_{\mathrm{mix}}U_{\mathrm{sc}}r^2w\right) = gr^2(\rho_{\mathrm{atm}}-\rho_{\mathrm{mix}}) - 2wpr\rho_{\mathrm{mix}}\sum_j w_{s,j}^{(0)}\Pi_j^{(0)}. \tag{37}$$

The equation for conservation of thermal energy writes as

$$\frac{\mathrm{d}}{\mathrm{d}s}\left(\rho_{\mathrm{mix}}U_{\mathrm{sc}}r^2C_{\mathrm{mix}}T\right) = 2r\rho_{\mathrm{atm}}U_{\epsilon}C_{\mathrm{atm}}T_{\mathrm{atm}} - r^2w\rho_{\mathrm{atm}}g - 2Tpr\rho_{\mathrm{mix}}\sum_j \left[C_{s,j}w_{s,j}\right]^{(0)}\Pi_j^{(0)} \tag{38}$$

GMDD
8, 3745–3790, 2015

and the equation for the variation rate of mixture specific heat in terms of the moments of the mass fraction distribution write as:

$$\frac{\partial C_{\text{mix}}}{\partial s} = \frac{1}{\rho_{\text{mix}} U_{\text{sc}} r^2} \left[C_{\text{atm}} 2 r \rho_{\text{atm}} U_\epsilon - C_{\text{mix}} \left(2 r \rho_{\text{atm}} U_\epsilon - 2 r p \rho_{\text{mix}} \sum_j w_{s,j}^{(0)} \Pi_j^{(0)} \right) \right.$$
$$\left. - 2 p r \rho_{\text{mix}} \sum_j \left[C_{s,j} w_{s,j} \right]^{(0)} \Pi_j^{(0)} \right]. \tag{39}$$

The formulation of the equations for the gas constant R_{g} and the coordinates of the (x, y, z) remain unchanged.

4 Numerical scheme

The plume rise equations are solved with a predictor-corrector Heun's scheme (Ascher and Petzold, 1998) that guarantees a second–order accuracy, keeping the execution time in the order of seconds. If we rewrite the system of ordinary differential equation with the following compact notation:

$$\frac{\partial y}{\partial s} = f(s, y), \qquad y(s_0) = y_0, \tag{40}$$

where y is the vector of the quantities in the left-hand sides of the conservation equations presented in the previous section, then the procedure for calculating the numerical solution by way of Heun's method (Süli and Mayers, 2003) is to first calculate the intermediate values $\widetilde{y}_{i+1}$ and then the solution y_{i+1} at the next integration point

$$\begin{aligned} \widetilde{y}_{i+1} &= y_i + \mathrm{d}s f(s_i, y_i), \quad \text{predictor step} \\ y_{i+1} &= y_i + \frac{\mathrm{d}s}{2} \left(f(s_i, y_i) + f(s_{i+1}, \widetilde{y}_{i+1}) \right) \quad \text{corrector step.} \end{aligned} \tag{41}$$

GMDD
8, 3745–3790, 2015

4.1 Quadrature method of moments

We observe that to calculate the right-hand side for both the predictor and corrector step we need not only the moments M^i, but also the additional moments $[w_s]^i$, $[w_s\rho_s]^i$ and $[w_s\rho_s C_s]^i$. As in Marchisio and Fox (2013), the integral in the definition of these moments is replaced by a quadrature formula and the moments, for a generic variable $\psi = \psi(D)$, are approximated as:

$$\psi^{(i)} = \frac{1}{M^{(i)}} \int_0^{+\infty} \psi(D) f(D) D^i \mathrm{d}D \approx \sum_{l=1}^{N} \psi(D_l) D_l^i \omega_l \tag{42}$$

Here ω_l and D_l are known as "weights" and "nodes" (or "abscissae") of the quadrature, respectively, and the accuracy of a quadrature formula is quantified by its degree. The degree of accuracy is equal to d if the interpolation formula is exact when the integrand is a polynomial of order less than or equal to d and there exists at least one polynomial of order $d+1$ that makes the interpolation formula inexact. In particular, an N-point Gaussian quadrature rule, named after Carl Friedrich Gauss, is a quadrature rule constructed to yield an exact result for polynomials of degree $2N-1$ or less by a suitable choice of the nodes D_l and weights ω_l for $l = 1, \ldots, N$.

The Wheeler algorithm, as presented in Marchisio and Fox (2013), provides an efficient $O(N^2)$ algorithm for finding a full set of weights and abscissas for a realizable moment set. The resulting nodes D_l are always within the support (and therefore represent realizable values of the particle size), and the weights ω_l are always positive, ensuring that, when the quadrature is used, accurate results are obtained. Nevertheless, these properties are respected only if the moment set is realizable, meaning that there exists a particle size distribution resulting in that specific set of moments. If the Wheeler algorithm is fed with invalid moment sets, unrealizable nodes can be calculated, jeopardizing the stability of the simulation.

A strategy that might overcome the problem of moment corruption is replacing unrealizable moment sets as soon as they appear. An algorithm of this kind was developed

GMDD
8, 3745–3790, 2015
PLUME-MoM
M. de' Michieli Vitturi et al.

by McGraw (McGraw, 2006). The algorithm first verifies whether the moment set is realizable (by looking at the second-order difference vector or by looking at the Hankel-Hadamard determinants). If the moment set is unrealizable it proceeds with the correction. In the numerical model here presented, the implementation of the correction algorithm of Wright is derived from the version presented in Marchisio and Fox (2013).

Thus, for each integration step, the following steps are performed:

- the nodes $D_{j,l}$ and weights $\omega_{j,l}$ are calculated with the Wheeler algorithm for $l = 1, \ldots, N$;
- the quadrature formula (Eq. 42) is used to evaluate the moments $[w_s]_j^{(i)}$, $[w_s\rho_s]_j^{(i)}$ and $[w_s\rho_s C_s]_j^{(i)}$;
- the right-hand side of the ODE's system (Eq. 40) is evaluated explicitly;
- the solution is advanced with the predictor (or the corrector) step of the Heun's scheme;
- for each particles family j, the moments $M_j^{(i)}$ $(i = 0, \ldots, 2N-1)$, if required, are corrected with the McGraw (or Wright) algorithm.

We observe that if the jth family of particles is monodisperse with diameter $\overline{d}_j$, the Wheeler algorithm fed with the first two moments only gives as result a single quadrature node $D_{j,1} = \overline{d}_j$ with weight $\omega_{j,1} = 1$. This allows us also to use the model for the simplified case where the solid particle distribution is partitioned in a finite number of classes with constant size, assigning to each class a monodisperse distribution.

4.2 Initial condition

Initial conditions at the vent include the initial plume radius (r_0), mixture velocity ($U_{sc,0}$) and temperature (T_0), gas mass fraction (n_0) and the particles size distribution through

GMDD
8, 3745–3790, 2015

the initial moments $M_0^{(i)}$. The initial moments are evaluated analytically according to the particle size distribution, as described below.

4.2.1 Lognormal distribution

For the application presented in this work, the initial distribution $f(D)$ at the base of the plume is defined as a function of the particles diameter expressed in meters (m), in order to give a corresponding normal distribution with parameters μ and σ for the mass concentration expressed as a function of the Krumbein phi (ϕ) scale (when all the particles have the same density).

Given the parameters μ and σ, the initial distribution then writes as:

$$f(D) = \frac{6C_0}{(-\sigma \log 2)\, D^4 \sqrt{2\pi^3}} e^{-\frac{[-\log(1000D)-\mu \log 2]^2}{2(\sigma \log 2)^2}}. \tag{43}$$

where C_0 is a parameter that has to be chosen in order to satisfy the condition on the initial mass (or volume) fraction of particles.

We observe that if we introduce the following re-scaled variables for the diameter, the mean and the variance:

$$\overline{D} = 1000D, \quad \overline{\mu} = -\mu \log 2, \quad \overline{\sigma} = -\sigma \log 2, \tag{44}$$

then it is possible to rewrite the particle distribution $f(D)$ in terms of a lognormal distribution in the variable $\overline{D}$ with parameters $\overline{\mu}$ and $\overline{\sigma}$:

$$\overline{f}(\overline{D}) = \frac{6 \cdot 10^{12} C_0}{\pi \overline{D}^3} \frac{1}{\overline{\sigma}\overline{D}\sqrt{2\pi}} e^{-\frac{\left[\log(\overline{D})-\overline{\mu}\right]^2}{2\overline{\sigma}^2}} = \frac{6 \cdot 10^{12} C_0}{\pi \overline{D}^3} \text{lognorm}\,(\overline{D}, \overline{\mu}, \overline{\sigma}). \tag{45}$$

GMDD
8, 3745–3790, 2015

Consequently, we can evaluate the moments $M^{(i)}$ of $f(D)$ analytically from the moments of the lognormal distribution as:

$$M^{(i)} = \frac{6C_0}{\pi} 10^{3(3-i)} \exp\left[(i-3)\overline{\mu} + \frac{1}{2}(i-3)^2\overline{\sigma}^2\right], \tag{46}$$

and we obtain, from the third moment:

$$M^{(3)} = \frac{6C_0}{\pi} \Rightarrow C_0 = \alpha_s^0 \tag{47}$$

where α_s^0 is the initial volume fraction of the particles in the solid-gas mixture.

From the expressions of the moments it follows also that, if the mass concentration expressed as a function of the Krumbein scale has a lognormal distribution, the Sauter mean diameter D_A expressed in meters can be evaluated as

$$D_A = L_{32} = \frac{M^{(3)}}{M^{(2)}} = 10^{-3} \exp\left(\overline{\mu} - \frac{1}{2}\overline{\sigma}^2\right), \tag{48}$$

or, if expressed in ϕ, as

$$D_A^{\phi} = L_{32}^{\phi} = \mu + \frac{1}{2}\sigma^2 \log(2). \tag{49}$$

We observe that processes involving the mutual interaction between particles and the interaction between the particles and the carrier fluid (friction and cohesion between the particles; viscous drag; chemical reactions between fluid and solid components) operate at the surface of the particles. For this reason the Sauter mean diameter, based on the specific area of the particles, play a major role and it is important to remark that it differs from the mean μ of the lognormal distribution by a factor proportional to the variance σ^2. For numerical models describing the multiphase (particulate) nature of the matter and which approximate the particle size distribution with an average size,

GMDD
8, 3745–3790, 2015
PLUME-MoM
M. de' Michieli Vitturi et al.

it is hence more appropriate to use, as particle size representative of a lognormal distribution, the Sauter mean diameter than the mean diameter μ. The difference between the two approximations is smaller the narrower the particle size distribution. We must also remark that, while for particles in the inertial-dominated regime (e.g. $\mathrm{Re}_p > 2000$) Loth et al. (2004) showed that the Sauter mean diameter is the effective diameter, regardless of particle shape, particle size distribution, particle density distribution or net volume fraction, for particles in the creeping flow regime ($\mathrm{Re}_p \ll 1$) the effective mean diameter is the volume-width diameter.

When the Sauter mean diameter is used, also the variance and the SD should be based on the specific surface area (Rietema, 1991). Hence:

$$\sigma_A^2 = \int_0^{+\infty} \left(\frac{1}{D} - \frac{1}{D_A}\right)^2 \frac{\pi}{6} D^3 f(D) \mathrm{d}D, \tag{50}$$

or, expressed as a function of the moments:

$$\sigma_A^2 = \frac{M^{(1)} M^{(3)} - (M^{(2)})^2}{(M^{(3)})^2}. \tag{51}$$

Finally, we observe that if the mass concentration expressed as a function of the Krumbein scale has a lognormal distribution and both the Sauter mean diameter $L_{32} = M^{(3)}/M^{(2)}$ and the mean particle length averaged with respect to particle number density $L_{10} = M^{(1)}/M^{(0)}$ (or if the first 4 moments) are known then we can solve for the re-scaled mean and variance $\overline{\mu}$ and $\overline{\sigma}$ the following system:

$$\begin{cases} L_{10} = 10^{-3} \exp\left(\overline{\mu} - \frac{5}{2}\overline{\sigma}^2\right) \\ L_{32} = 10^{-3} \exp\left(\overline{\mu} - \frac{1}{2}\overline{\sigma}^2\right) \end{cases} \tag{52}$$

Once the re-scaled mean and variance are known, we can obtain μ and σ in the Krumbein ϕ scale.

GMDD
8, 3745–3790, 2015

When the initial distribution is expressed for the mass fractions instead of the particle number, and the mass fraction written as a function of the Krumbein scale has a normal distribution with mean μ and variance σ^2, then we can express the continuous distribution as

$$\varphi(\phi) = \frac{K_0}{\sigma\sqrt{2\pi}} e^{-\frac{(\phi-\mu)^2}{2\sigma^2}}, \tag{53}$$

where K_0 is a parameter that has to be chosen in order to satisfy the condition on the initial mass fraction of particles. We observe that this expression of the distribution is not based on the assumption of constant density for the particles of different size.

In this case, the moments $\Pi^{(i)}$ are given by the following expression

$$\Pi^{(i)} = K_0 \sum_{j=0}^{\lceil i/2 \rceil} \binom{i}{2j} (2j-1)!!\sigma^{2j}\mu^{i-2j}. \tag{54}$$

where the symbol "!!" denotes the double factorial.

Now, being the 0-th moment equal to the mass fraction of particles, we obtain $K_0 = x_s$. Furthermore, we observe that the mass fraction averaged diameter in the ϕ scale is given by the ratio $\Pi^{(1)}/\Pi^{(0)}$, while the variance of the mass fraction distribution can be evaluated as $\left[\Pi^{(2)}\Pi^{(0)} - (\Pi^{(1)})^2\right]/(\Pi^{(0)})^2$. These two quantities correspond to the parameters (μ, σ^2) generally used to describe the mass fraction when a normal distribution in the ϕ scale is assumed. For this reason, when we want to track the changes of the mass fraction averaged diameter and its SD (or variance) in the ϕ scale during the plume rise, it is preferred to use a formulation based on the moments $\Pi^{(i)}$ than the moments $M^{(i)}$.

GMDD
8, 3745–3790, 2015

5 Application

5.1 Simulation inputs

We applied the model to three different test cases with different vent and atmospheric conditions:

- Test Case 1 – weak plume without wind;
- Test Case 2 – weak plume with wind;
- Test Case 3 – strong plume.

The parameters used for the different test cases are listed in Table 1, while the atmospheric conditions are plotted in Fig. 3. For the weak plumes a mass flow rate of 1.5×10^6 Kg s^{-1} has been fixed, while for the strong plume the value is 1.5×10^9 Kg s^{-1}. The temperature pressure and density profiles used for the test case without wind (Test Case 1) are those defined by the International Organization for Standardization for the International Standard Atmosphere, while the profiles for the other two test cases come from reanalysis data.

For all the runs presented here, a single family of particles has been used, with a normal distribution (with parameters μ and σ) for the mass concentration as a function of the diameter expresses in the ϕ scale and with density varying according to Eq. (3).

We first present a comparison of the plume profiles obtained with the 3 different descriptions presented in the previous sections and highlighted in the three colored boxes of Fig. 2 for the Test Case 2: method of moments for the particle number being function of the size expressed in meters; method of moments for the particle mass fraction being function of the size expressed in the ϕ scale; discretization in uniform bins in the ϕ scale. For this comparison, the mass flow rate at the vent is 1.5×10^6 Kg s^{-1} and a rotating wind is present, as shown in Fig. 3, while the mean and the SD of the initial total grain size distribution are respectively 2 and 1.5, expressed in the ϕ scale. The results of the numerical simulations obtained with the three different formulations are

GMDD
8, 3745–3790, 2015

presented in Fig. 4 and they perfectly match, showing that the method of moments (dotted lines), both applied to the continuous distribution of the particles number (red) or to the mass distribution (green), gives the same results of the classical formulation based on the discretization of the mass distribution in bins (solid line). For these simulations, we used only the first 6 moments of the distributions, while 13 bins have been employed with the discretized formulation. This results in a smaller number of equations to solve for the method of moments and, despite the additional cost of the method of moments due to the evaluation of the quadrature points and formulas through the Wheeler algorithm, in a smaller computational time, with a gain of about 30 %.

5.2 Simulation results

In this section we want to study the variation during the ascent of solid mass flux (due to particles settling) and of the mean and the variance of the mass distribution along the column. As shown in the previous section, there are no significant differences in the results obtained with the three different descriptions of the grain size distribution. For this reason, in the following we restrict the analysis only to the formulation based on the moments of the mass fraction distribution as a function of the diameter expressed in the ϕ scale. With this approach, the mean, the variance and the skewness of the mass distribution along the column are easily obtained from the first 4 moments $\Pi^{(i)}$ of the mass fraction distribution.

In Fig. 5 we present the results relative to the Test Case 2 for an initial particle size distribution with mean diameter 2 and SD 1.5, expressed in the ϕ scale. In the left and middle panels the mean, the variance and the skew of the mass fraction distribution are shown respectively, while in the right panel the cumulative loss of solid mass flux is plotted as a percentage of the initial value. We observe a decrease in the mean size of the particles, due to the different settling velocities of particles of different sizes. A decrease in the variance of the size distribution with height is also observed from the second plot. We remark that the particles have a normal distribution only at the base of the column (resulting in a null skewness), and the negative skew at the top of

GMDD
8, 3745–3790, 2015

the column indicates that the tail on the left side of the grain size distribution is longer than the tail on the right side, i.e. the mass is more concentrated on the right of the spectrum of particle sizes (finer particles). For this reason we do not have to look at the mean and the variance plotted in Fig. 5 as the parameters of a normal (and symmetric) distribution. Nonetheless the changes in the mean, the variance and the skewness, we remark that these changes are quite small and for this reason the parameters of the total grain size distribution at the top of the eruptive column can be assumed to be a good approximation of the parameters at the base of the column, and vice versa. However, this is true for the specific input condition of this test case and not in general. For this reason, it is important to quantify the uncertainty of this assumption for different initial total grain size distributions and different atmospheric conditions.

5.3 Uncertainty and sensitivity analysis

When dealing with volcanic processes and volcanic hazards, our understanding of the physical system is limited, and vent parameters (volatile contents, temperature, grain size distribution, etc.) are not always well-constrained or are constrained with significant uncertainty. These factors mean that it is difficult to predict the characteristic of the ash cloud released from the volcanic column with certainty. The best alternative is to quantify the probability of the outcomes (for example the grain size distribution at the top of the column) by coupling deterministic numerical codes with stochastic approaches. It is our goal in this work also to assess the ability to systematically quantify the uncertainty and the sensitivity of the plume model outcomes to uncertain or variable input parameters, in particular to those characterizing the grain size distribution at the base of the eruptive column.

Uncertainty quantification (UQ) or nondeterministic analysis is the process of characterizing input uncertainties, propagating forward these uncertainties through a computational model, and performing statistical or interval assessments on the resulting responses. This process determines the effect of uncertainties on model outputs or results. In particular, in this work we wanted to investigate for different test cases the

GMDD
8, 3745–3790, 2015

uncertainty in four response functions (plume height, solid mass flux lost and mean and variance of the mass fraction distribution at the top of the eruptive column) when the mean and the SD of the distribution at the base are random variables with a uniform probability distribution in the space $(\mu, \sigma) \in [-1; 3] \times [0.5; 2.5]$.

In volcanology Monte Carlo simulations are frequently used to perform uncertainty quantification analysis. These methods rely on repeated random sampling of input parameters to obtain numerical results; typically one runs simulations many times over in order to obtain the distribution of an unknown output variable. The cost of the Monte Carlo method can be extremely high in terms of number of simulations to run, and thus several alternative approach have been developed. Latin hypercube sampling is another sampling technique for which the range of each uncertain variable is divided into N_s segments of equal probability, where N_s is the number of samples requested. The relative lengths of the segments are determined by the nature of the specified probability distribution (e.g., uniform has segments of equal width, normal has small segments near the mean and larger segments in the tails). For each of the uncertain variables, a sample is selected randomly from each of these equal probability segments. These N_s values for each of the individual parameters are then combined in a shuffling operation to create a set of N_s parameter vectors with a specified correlation structure. Compared to Monte Carlo sampling, the Latin hypercube sampling has the advantage that in the resulting sample set every row and column in the hypercube of partitions has exactly one sample, and thus a smaller number of samples is required to cover all the parameter space. In the left panel of Fig. 6 an example of Latin hypercube sampling with $N_s = 10$ and a uniform distribution probability for both μ and σ is plotted.

An alternative approach to uncertainty quantification is the so-called generalized Polynomial Chaos Expansion method (gPCE), a technique that mirrors deterministic finite element analysis utilizing the notions of projection, orthogonality, and weak convergence. PCE was developed by Norbert Wiener in 1938 and it soon become widely used because of its efficiency when compared to Monte Carlo simulations. The term "Chaos" here simply refers to the uncertainties in input, while the word "Polynomial"

GMDD
8, 3745–3790, 2015

is used because the propagation of uncertainties is described by polynomials. If ζ is the vector of uncertain input variables, the aim of the gPCE is to express the output function Y in the form of a polynomial γ as follows:

$$\gamma(\zeta) = \gamma_0 + \gamma_1 P_1(\zeta) + \gamma_2 P_2(\zeta) + \ldots + \gamma_3 P_3(\zeta) \tag{55}$$

where P_i are polynomials which form an orthogonal basis. The choice of the polynomials basis depends on the probability distribution of the input variables. In particular, for a uniform distribution, the basis of the expansion is given by the Lagrange polynomials. For the application presented in this work the coefficients of the expansion have been evaluated using a spectral projection where the computation of the required multi-dimensional integrals is based on the tensor product of one-dimensional Gaussian quadrature rules. In order to compute the quadrature points, the grid used in our work is the Clenshaw–Curtis grid (Fig. 6, right), representing a good solution for a multi-dimensional Gaussian quadrature with a small number of variables.

We present here the results of several tests performed coupling the plume model with the Dakota toolkit (Adams et al., 2013) to investigate systematically the capability of the LHS and the gPCE techniques to assess the uncertainty in four response functions (plume height, solid mass flux lost and mean and variance of the mass fraction distribution at the top of the eruptive column) when the mean and the variance at the base are unknown. For all the test cases two sets of 1000 and 2000 simulations have been performed for the LHS, and the results have been compared with those obtained with three tests for the gPCE and respectively 9, 36 and 91 simulations performed for the multi-dimensional quadrature. In order to compare the results, the cumulative distributions of the four response functions have been plotted in Fig. 7 for Test Case 1 (no wind). On the x axes we can see the range of the values obtained for the response functions: −1–3.5 for the mean of the TGSD at top of the column expressed in the ϕ scale; 0.4–2.2 for the SD; 10.41–10.47 km for the column height and 10–60 % for the percentage of solid mass flux lost. All the uncertainty quantification tests produced very similar results, with a small difference in the cumulative distribution observed only

GMDD
8, 3745–3790, 2015

in the distribution of the solid mass flux lost obtained with the gPCE technique and 9 and 36 quadrature points. Similar results have been obtained for the other Test Cases (not shown here). Thus, the results highlights that gPCE represents a valid alternative to Monte Carlo simulations, with a number of runs required to produce the same accuracy reduced by a factor 10 (91 simulations vs. 1000 simulations).

As mentioned previously, the aim of the gPCE is to express the output of the models as polynomials and these polynomials can be used to obtain response surfaces for the output parameters as functions of the unknown input parameters. In the four bottom panels of Fig. 7 the contours of the four response surfaces for the output investigated in this work have been plotted, showing the dependence on the uncertain input parameters. The mean and the SD of the TGDS at the top of the eruptive column clearly reflects the corresponding values at the bottom, with a small effect on the mean size at the top of larger values of the bottom SD, resulting in an increase in the average grain size (see the curves in the first panel bending on the left for higher values of σ). Conversely, the plume height for this test case shows a non-linear dependency but at the same time a small sensitivity to the initial grain size distribution, with changes smaller than 1 % of the average height. This can be explained by the fact that a large amount of air is entrained in the column during the ascent and the contribution of the solid fraction to the overall dynamics becomes small compared to that exerted by the gas. Finally, we observe that the loss of particles is mostly controlled by mean size of the TGSD.

In Fig. 8 the same contour plots are shown for the polynomial expansion computed for Test Case 2 (top) and Test Case 3 (bottom) with 91 quadrature points. The results show again that the total grain size distribution at the base of the vent represents a reasonable approximation of that at the top of the column. For these test cases, both the column height and the solid mass lost appear to be mostly controlled by the mean size of the TGSD at the base of the column, with a small sensitivity of the height to the initial grain size distribution. We also observe that the maximum percentage of loss in the solid mass flux is about 15 % for the strong plume simulations, and it is attained for larger mean sizes and smaller dispersion of the initial TGSD. This value is noticeably

GMDD
8, 3745–3790, 2015

smaller than that obtained for the weak bent test case (≈ 40 %) and for the weak test case without wind (≈ 60 %). Despite the loss of particles, in both the cases the range of variation of the column height is quite small and, as previously mentioned, this is due to the large amount of air entrained in the volcanic column that reduce the contribution of the solid fraction to the overall dynamics. As an example to understand the relvance of the entrained aid, for a simulation performed for the weak plume without wind and with $\mu = 2$ and $\sigma = 1.5$ in the ϕ scale, the mass flow rate at the top of the column is $1.2 \times 10^8\,\mathrm{Kg\,s^{-1}}$, compared to the value at the base of $1.5 \times 10^6\,\mathrm{Kg\,s^{-1}}$.

5.4 Sensitivity analysis

With the polymomial chaos expansion it is also possible to easily obtain the variance-based sensitivity indices with no additional computational cost. In contrast with some instances, where the term sensitivity is used in a local sense to denote the computation of response derivatives at a point, here the term is used in a global sense to denote the investigation of variability in the response functions. In this context, variance-based decomposition is a global sensitivity method that summarizes how the variability in model output can be apportioned to the variability in individual input variables (Adams et al., 2013). This sensitivity analysis uses two primary measures, the main effect sensitivity index S_i and the total effect index T_i. These indices are also called the Sobol indices. The main effect sensitivity index corresponds to the fraction of the uncertainty in the output, Y, that can be attributed to input x_i alone. The total effects index corresponds to the fraction of the uncertainty in the output, Y, that can be attributed to input x_i and its interactions with other variables. The main effect sensitivity index compares the variance of the conditional expectation $\mathrm{Var}_{x_i}[E(Y|x_i)]$ against the total variance $\mathrm{Var}(Y)$. Formulas for the indices are:

$$S_i = \frac{\mathrm{Var}_{x_i}\left[(Y|x_i)\right]}{\mathrm{Var}(Y)} \tag{56}$$

GMDD
8, 3745–3790, 2015
PLUME-MoM
M. de' Michieli Vitturi et al.

and

$$T_i = \frac{E(\mathrm{Var}(Y|X_{-i}))}{\mathrm{Var}(Y)} \tag{57}$$

where $Y = f(x)$ and $x_{-1} = (x_1, \ldots, x_{i-1}, x_{i+1}, \ldots, x_m)$. Similarly, it is also possible to define the sensitivity indices for higher order interactions such as the two-way interaction $S_{i,j}$. The calculation of S_i and T_i requires the evaluation of m-dimensional integrals which are typically approximated by Monte-Carlo sampling. However, in stochastic expansion methods, it is possible to obtain the sensitivity indices as analytic functions of the coefficients in the stochastic expansion.

The results of the sensitivity analysis for the four outputs and the three test cases investigated are presented in the bar plot of Fig. 9. For each of the four groups (one for each of the different output functions) the three bars represent the main sensitivity indices for the three test cases (test 1 on the left, test 2 in the middle and test 3 on the right) while the different colors are for the sensitivity indices with respect to different variables (blue is for the mean of the initial TGSD, green for the standard variation and brown for the 2nd order coupled interaction). Again, the sensitivity analysis confirms that the mean and the SD of the grain size distributions at the top of the eruptive column are controlled by the respective parameters of at base of the column. The mean of the TGSD also controls the percentage of solid mass flux lost during the rise of the column and the plume height for the two test cases with wind, while for the weak test case without wind the dispersion of the distribution and second-order interaction also play a major role in controlling plume height variability. However, as already observed with the uncertainty quantification analysis, we remark that the variability in the plume height, when the mean and the SD of the TGSD vary in the investigated ranges, is extremely small for all the test cases (less than 1 % with respect to the average values) and thus the investigation of how the variability in model output can be apportioned to the variability in individual input variables is less relevant for the plume height than for the other output parameters.

GMDD
8, 3745–3790, 2015

6 Conclusions

In this work we have presented an extension, based on the method of moments, of the Eulerian steady-state volcanic plume model presented in Barsotti et al. (2008) (derived from Bursik, 2001). Two different formulations, one based on a continuous distribution of the number of particles as a function of the size and a second based on the continuous distribution of the mass fraction, have been presented. The tracking of the moments of mass distribution, defined as a function of the Krumbein phi scale, has the advantage that with the first three moments only we are able to recover the mean and the SD of the total grain size distribution. The results of a comparison between the two formulations based on the method of moments and the classical formulation based on the discretization of the mass distribution in bins show that the different approaches produce the same results, with an advantage of the method of moments in terms of computational costs. Furthermore, a formulation based on continuous description of particle size, is better suited to properly describe additional processes such as aggregation.

An uncertainty quantification analysis has also been applied to the formulation based on the moments of the mass distribution. The results show for all the test cases a small change of the mean and variance of the particle mass distribution along the column, indicating that the total grain size distribution at the base of the vent represents a reasonable approximation of that at the top of the column. Furthermore, based on the plume model assumptions and outcomes, we observe a small sensitivity of the plume height to the initial grain size distribution, with variations of the order of tens of meters.

The comparison between the latin hypercube sampling technique and the generalized polynomial chaos expansion method shows that the latter only requires 91 simulations to produce the same results, in terms of cumulative probability distributions of several output, obtained with 1000 simulations and the LHS. In fact, the full uncertainty quantification analysis performed on a High Performance Computing 48 multi core Shared Memory system (HPC-SM) at Istituto Nazionale di Geofisica e Vulcanolo-

GMDD
8, 3745–3790, 2015

gia (INGV), section of Pisa, Italy, required less than 2 s for the gPCE method with 91 quadrature points. These results make the new numerical code presented here, coupled with the uncertainty technique investigated, well-suited for real time hazard assessment.

Code availability

The source code with the input files for some simulation presented in this work are available for download on the Volcano Modelling and Simulation gateway (http://vmsg.pi.ingv.it/) and on the site for collaborative volcano research and risk mitigation Vhub (https://vhub.org/).

Acknowledgements. The authors are grateful to Samantha Engwell for the helpful discussion and suggestions on the application of the model. This work has been partially supported by the project MEDiterranean SUpersite Volcanoes (MED-SUV) FP7 ENV.2012.6.4-2 Grant agreement no. 308665 (European Community).

References

Adams, B. M., Bauman, L. E., Bohnhoff, W. J., Dalbey, K. R., Ebeida, M. S., Eddy, J. P., Eldred, M. S., Hough, P. D., Hu, K. T., Jakeman, J. D., Swiler, L. P., and Vigil, D. M.: DAKOTA, A Multilevel Parallel Object-Oriented Framework for Design Optimization, Parameter Estimation, Uncertainty Quantification, and Sensitivity Analysis: Version 5.4 User's Manual, Sandia Technical Report SAND2010-2183, December 2009, updated April 2013, 2013. 3773, 3775

Ascher, U. M. and Petzold, L. R.: Computer methods for ordinary differential equations and differential-algebraic equations, Siam, 61, 1998. 3762

Barsotti, S., Neri, A., and Scire, J.: The VOL-CALPUFF model for atmospheric ash dispersal: 1. Approach and physical formulation, available at: www.agu.org/pubs/crossref/2008/2006JB004623.shtml (last access: 30 April 2015), J. Geophys. Res., 113, B03208, doi:10.1029/2006JB004623, 2008. 3747, 3752, 3756, 3777

Bonadonna, C. and Phillips, J.: Sedimentation from strong volcanic plumes, J. Geophys. Res., 108, 2340, doi:10.1029/2002JB002034, 2003. 3750

Briggs, G. A.: Plume rise predictions, in: Lectures on Air Pollution and Environmental Impact Analyses, edited by: Hangen, D. A., American Meteorological Society, Boston, MA, 59–111, 1975. 3757

Bursik, M.: Effect of wind on the rise height of volcanic plumes, Geophys. Res. Lett, 18, 3621–3624, 2001. 3747, 3755, 3757, 3760, 3777

Carneiro, J. N. E.: Development of a Presumed Function Method of Moments with Application to Polydisperse Sprays, Ph.D. thesis, Technische Universität München, Munich, Germany, 2011. 3750

Ernst, G. G., Sparks, R. S. J., Carey, S. N., and Bursik, M. I.: Sedimentation from turbulent jets and plumes, J. Geophys. Res., 101, 5575–5589, doi:10.1029/95JB01900, 1996. 3755

Glaze, L. S. and Baloga, S. M.: Sensitivity of buoyant plume heights to ambient atmospheric conditions: Implications for volcanic eruption columns, J. Geophys. Res., 101, 1529–1540, 1996. 3760

Hazewinkel, M.: Moment, Encyclopedia of Mathematics, Springer, ISBN 978-1-55608-010-4, 2001. 3749

Hulburt, H. M. and Katz, S.: Some problems in particle technology: a statistical mechanical formulation, Chem. Eng. Sci., 19, 555–574, 1964. 3747

Loth, E., O'Brien, T., Syamlal, M., and Cantero, M.: Effective diameter for group motion of polydisperse particle mixtures, available at: http://www.sciencedirect.com/science/article/pii/S0032591004001895 (last access: 30 April 2015), Powder Technol., 142, 209–218, 2004. 3767

Marchisio, D. L. and Fox, R. O.: Computational Models for Polydisperse Particulate and Multiphase Systems, Cambridge University Press, New York, 2013. 3763, 3764

Marchisio, D. L., Vigil, R. D., and Fox, R. O.: Quadrature method of moments for aggregation–breakage processes, J. Colloid Interf. Sci., 258, 322–334, 2003. 3747

McGraw, R.: Correcting Moment Sequences for Errors Associated with Advective Transport, available at: http://www.ecd.bnl.gov/pubs/momentcorrection_mcgraw2006.pdf (last access: 30 April 2015), 2006. 3764

Morton, B.: Forced plumes, J. Fluid Mech., 5, 151–163, 1959. 3757

Pfeiffer, T., Costa, A., and Macedonio, G.: A model for the numerical simulation of tephra fall deposits, J. Volcanol. Geoth. Res., 140, 273–294, doi:10.1016/j.jvolgeores.2004.09.001, 2005. 3752

Rietema, K.: The Dynamics of Fine Powders, Springer, the Netherlands, 1991. 3767

Süli, E. and Mayers, D. F.: An Introduction to Numerical Analysis, Cambridge University Press, Cambridge, UK, 2003. 3762

Textor, C., Graf, H., Herzog, M., Oberhuber, J., Rose, W. I., and Ernst, G.: Volcanic particle aggregation in explosive eruption columns. Part II: Numerical experiments, avialable at: http://www.sciencedirect.com/science/article/pii/S0377027305002994 (last access: 30 April 2015), J. Volcanol. Geoth. Res., 150, 378–394, 2006a. 3752

Textor, C., Graf, H.-F., Herzog, M., Oberhuber, J. M., Rose, W. I., and Ernst, G. G.: Volcanic particle aggregation in explosive eruption columns. Part I: Parameterization of the microphysics of hydrometeors and ash, available at: http://www.sciencedirect.com/science/article/pii/S0377027305002982 (last access: 30 April 2015), J. Volcanol. Geoth. Res., 150, 359–377, 2006b. 3752

Weil, J.: Plume rise, in: Lectures on Air Pollution Modelling, edited by: Venkatram, A. and Wyngaard, J. C., American Meteorological Society, Boston, MA, 119–166, 1988. 3757

Woods, A. W.: The fluid dynamics and thermodynamics of eruption columns, available at: http://www.springerlink.com/index/G4M430TG5X2H9J28.pdf (last access: 30 April 2015), B. Volcanol., 50, 169–193, 1988. 3760

Wright, S. J.: Buoyant jets in density-stratified crossflow, J. Hydraul. Eng., 110, 643–656, 1984. 3757

GMDD
8, 3745–3790, 2015

Table 1. Input parameters used for the numerical simulations. Vent height is the elevation of the base of the column above sea level. The values $\rho_{1,2}$ and $D_{1,2}$ are used to compute the density of the particles as a function of the diameter, according to Eq. (3). The values reported for μ and σ define the range used for the uncertainty quantification and sensitivity analysis.

Parameters	Units	Test Case 1	Test Case 2	Test Case 3
Radius	m	27	27	708
Velocity	$m\,s^{-1}$	135	135	275
Temperature	K	1273	1273	1053
Gass Mass Fraction		0.03	0.03	0.05
Vent Height	m	1500	1500	1500
ρ_1	$kg\,m^{-3}$	2000	2000	2000
ρ_2	$kg\,m^{-3}$	2600	2600	2600
D_1	m	8×10^{-6}	8×10^{-6}	8×10^{-6}
D_2	m	2×10^{-3}	2×10^{-3}	2×10^{-3}
μ	ϕ	−1.0–3.0	−1.0–3.0	−1.0–3.0
σ	ϕ	0.5–2.5	0.5–2.5	0.5–2.5

GMDD
8, 3745–3790, 2015

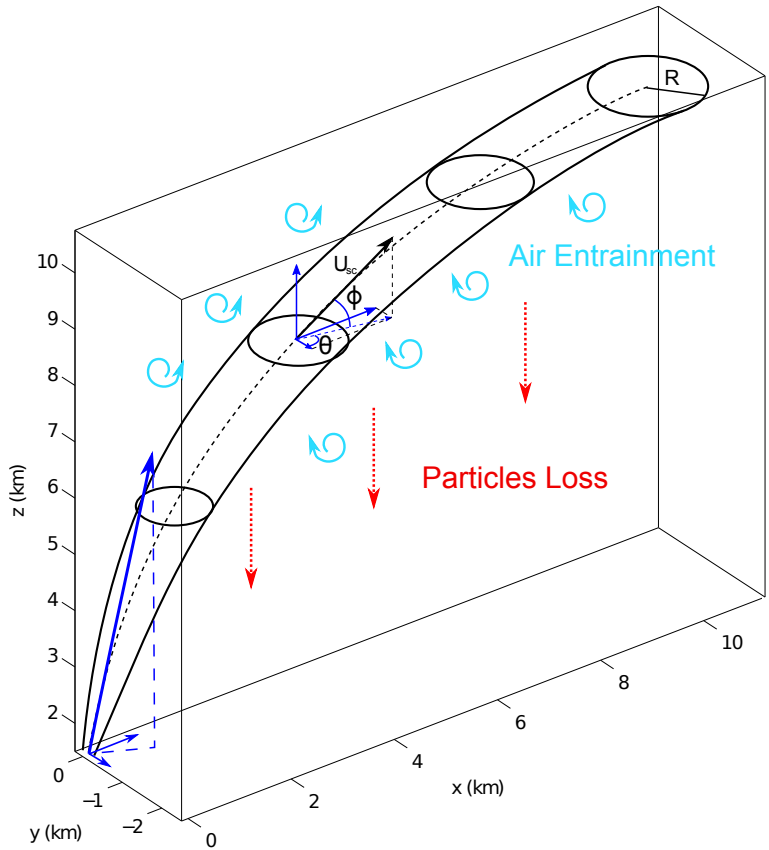

Figure 1. Schematic representation of the Eulerian plume model. The dashed black line represent the axis of the curvilinear coordinate *s*.

GMDD
8, 3745–3790, 2015

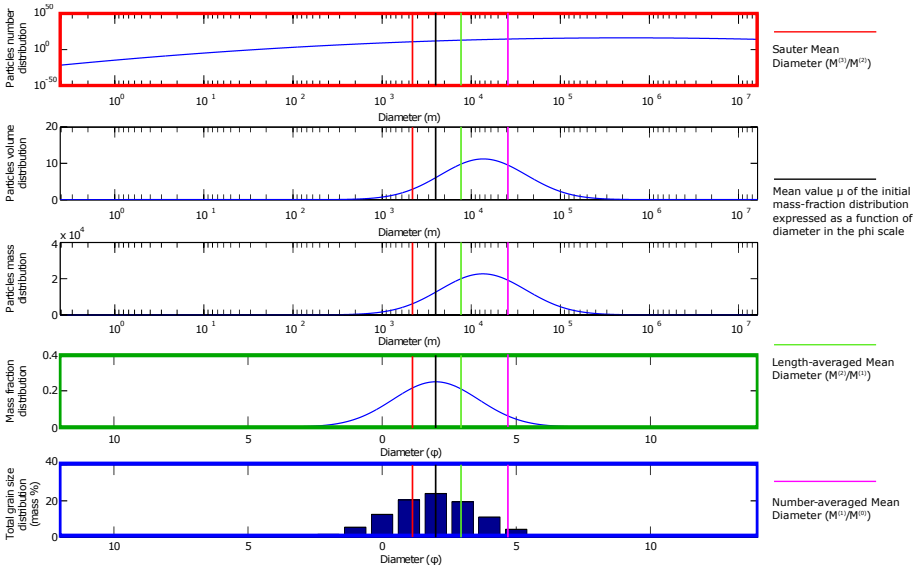

Figure 2. Visualization of a normal initial distribution in the Krumbein ϕ scale for the solid particles. On the top the particle number distribution expressed as a function of the diameter expressed in meters is plotted. On the second and third plots from the top the corresponding distributions of volume and mass are plotted, these two being different because the density is a function of the diameter. On the forth plot the continuous distribution (lognormal) of mass fraction as a function of the ϕ scale is plotted, while in the last plot the distribution has been discretized with 13 bins in the range $(-4; 8)$. On each panel different average radii are also plotted, together with the mean of the initial distribution. The first, fourth and fifth panel are highlighted with different color, also used in Fig. 4 for the solutions obtained with the three different representation of the initial grain size distribution.

GMDD
8, 3745–3790, 2015

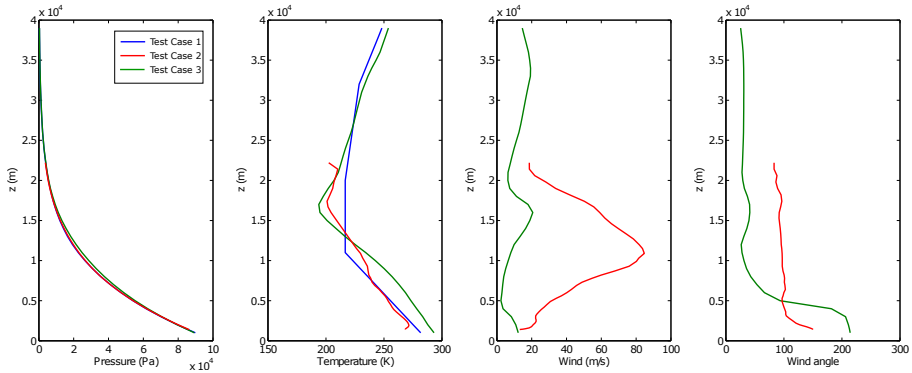

Figure 3. Atmospheric profiles for the three test cases. The height is expressed in m a.s.l. and for all the test cases the vent is located at 1500 m a.s.l. For the wind profiles only the profiles for the two test cases with wind are plotted.

GMDD
8, 3745–3790, 2015

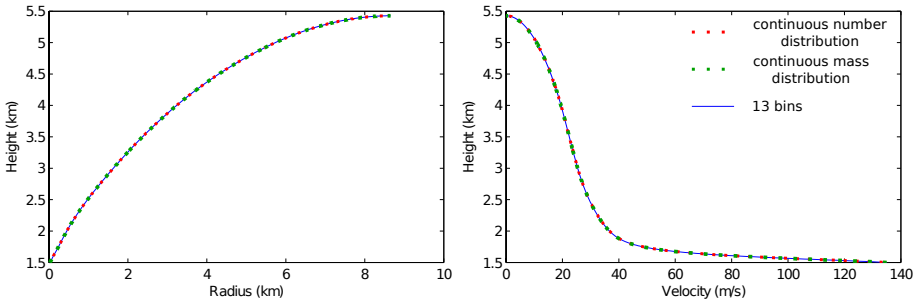

Figure 4. Height vs. radius (left) and velocity (right) for a weak plume, simulated with three different models. In blue the profiles obtained using 13 bins, in red the profiles obtained using a ocntinuous distribution of the particles number density and in green using a continuous distribution of the mass fraction.

GMDD
8, 3745–3790, 2015

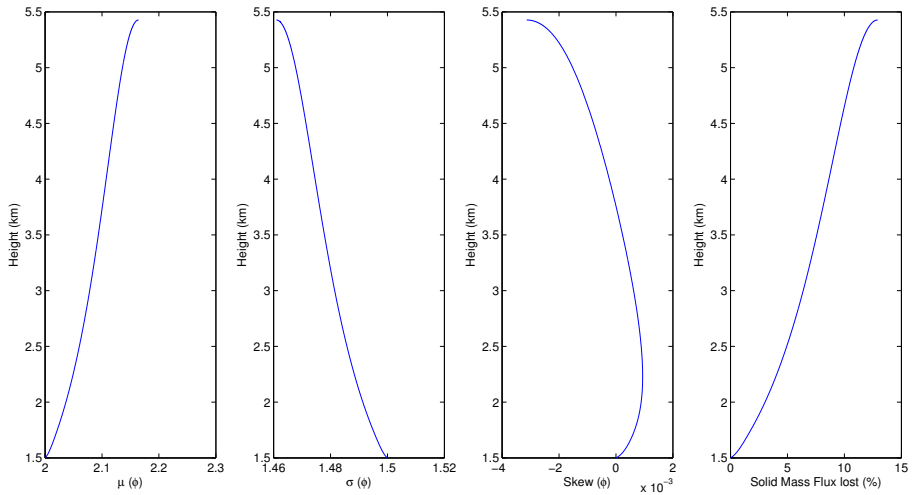

Figure 5. Particles distribution parameters (mean, variance and skewness) and cumulative loss of solid mass flux for the weak plume test case, simulated with the formulation based on the moments of the mass fraction distribution.

GMDD
8, 3745–3790, 2015

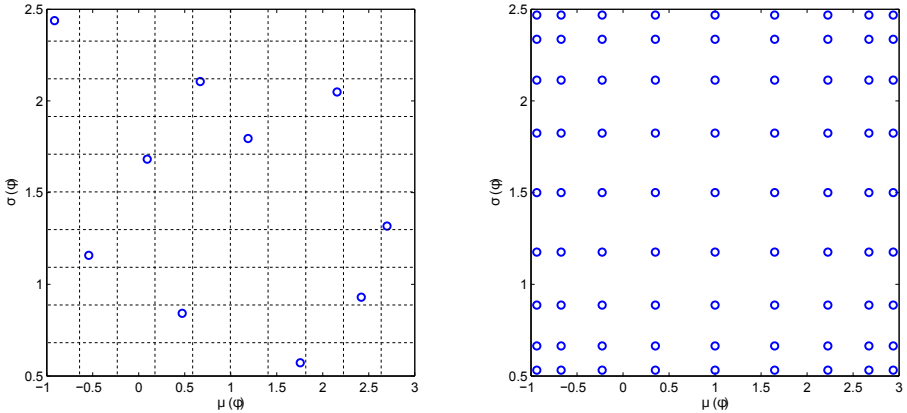

Figure 6. Two parameters Latin Hypercube Sampling with 10 points (left) and tensor product grid using 9 × 9 Clenshaw–Curtis points (right).

GMDD
8, 3745–3790, 2015

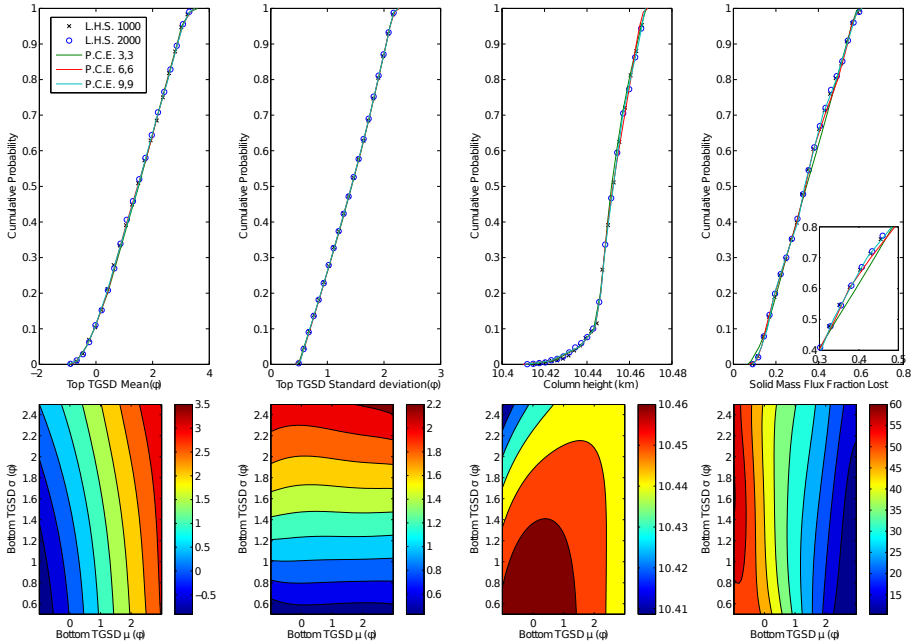

Figure 7. Cumulative distributions and response surfaces for test Case 1 (weak plume without wind). In the top panels the cumulative probability for several variables describing the outcomes of the simulations (mean and variance of the grain size distribution at the top of the column, column height and cumulative fraction of solid mass lost) are plotted for the uncertainty quantification analysis carried out with the two different techniques and for different numbers of simulations. The contour plots of the response functions of the four variables, obtained with the PCE with 91 quadrature points, are plotted in the bottom panels.

GMDD
8, 3745–3790, 2015

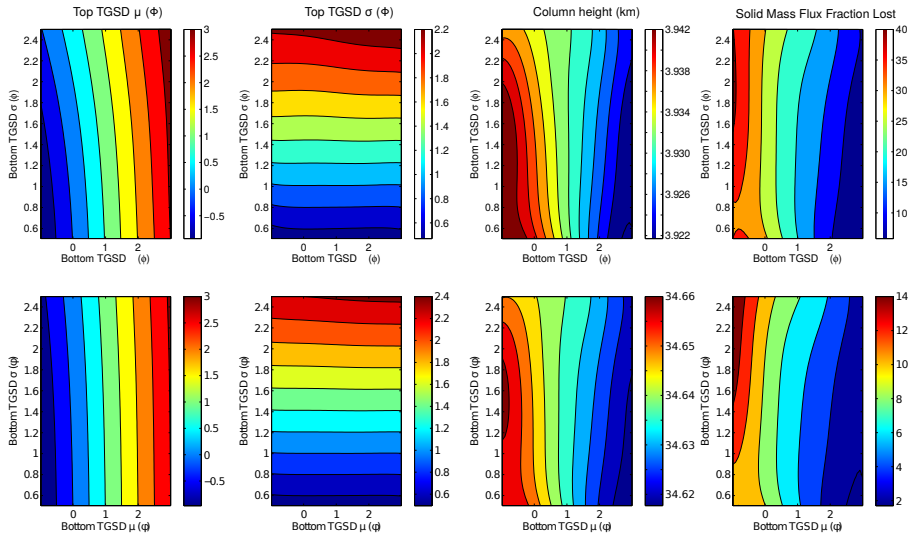

Figure 8. Response surfaces for Test Case 2 (weak plume with wind, 4 top panels) and Test Case 3 (strong plume with wind, 4 bottom panels) obtained with the PCE with 91 quadrature points. Please not that the color scale is not consistent between plots.

GMDD
8, 3745–3790, 2015

Figure 9. Sobol indices. For each of the four output parameters the three bars are for the different test cases: Test Case 1 on the left, Test Case 2 in the middle and Test Case 3 on the right. For each test case the different colors of the bars are for the different sensitivity indexes: blue for first order sensitivity index with respect to the the bottom TGSD mean, green for the bottom TGSD SD and brown for the second order combined sensitivity index.

GMDD
8, 3745–3790, 2015